Computer Assisted Mechanics and Engineering Sciences, 14: 107–125, 2007.

A numerical algorithm for obtaining an optimal temperature distribution in a 3D triple layered cylindrical skin structure

Le Zhang
Complex Biosystems Modeling Laboratory
Harvard-MIT(HST) Athinoula A. Matinos Center for Biomedical Imaging
Massachusetts General Hospital, Charlestown, MA 02129, USA

Weizhong Dai, Raja Nassar
Mathematics and Statistics, College of Engineering and Science
Louisiana Tech. University, Ruston, LA 71272, USA

(Received July 29, 2005)

In recent years, there has been interest in research related to hyperthermia combined with radiation and cytotoxic drugs to enhance the killing of tumors. The objective is to control laser heating of the tumor so that the temperature of the normal tissue surrounding the tumor remains low enough so as not to cause damage to the tissue. To achieve this objective, it is important to obtain an optimal temperature field of the entire treatment region. In this paper, we develop a numerical algorithm for obtaining an optimal temperature distribution in a 3D triple layered cylindrical skin structure by pre-specifying the temperatures to be obtained at the center and perimeter of the treated region on the skin surface. The method is comprised of designing a laser irradiation pattern, solving a 3D Pennes' bioheat equation by a numerical scheme, and optimizing the laser power.

NOMENCLATURE

C_l	specific heat of layer l
C_b^l	specific heat of blood in layer l
I	iterative index
$\mathbf{I}$	identity matrix
i, j, k	grid point
k_l	heat conductivity of layer l
L_l	depth of layer l
N_r , N_φ , N_l^z	numbers of grid points in the r, φ, z directions, respectively
n	time level
P_0	laser intensity
P_r^2	second order finite difference operator in the r direction
Q_r^l	heat source in layer l
R	radius of the skin structure
$Reff_l$	laser reflectivity in layer l
r, φ, z	cylindrical coordinates
S	least squares sum
T_l , T_b	tissue and blood temperatures, respectively
t	time
u_{ijk}^n	numerical solution

W_b^l	blood perfusion rate of layer l
α_l	laser absorptivity of layer 1
$\delta_z^2, \delta_\varphi^2$	second-order finite difference operators in the z, φ directions, respectively
ρ_l	density of layer l
σ	standard deviation of laser beam width
θ_l	tissue temperature elevation due to heating
$\Delta r, \Delta\varphi, \Delta z$	mesh sizes in the r, φ, z directions, respectively
Δt	time increment

1. Introduction

In recent years, there has been interest in research related to the hyperthermia combined with radiation and cytotoxic drugs to enhance the killing of tumors [15, 16, 24, 25, 30]. Conventional hyperthermia (target temperatures of 42–46°C) in conjunction with radiation has demonstrated increased effectiveness in the treatment of certain types of cancer, such as those of liver metastases [6, 16, 23]. The objective is to control laser heating of the tumor so that the temperature of the normal tissue surrounding the tumor remains low enough so as not to cause damage to the tissue. Thus, it is important to obtain a temperature field of the entire treatment region. With knowledge of the entire temperature field in the treatment region, clinical personnel can potentially control the heating source to deliver energy to the treatment target volume to raise its minimum temperature above 42°C, while limiting the temperatures in the normal tissue to prevent damage. However, it is not easy to obtain an accurate determination of the temperature field over the entire treatment region during clinical hyperthermia treatments, because the number of invasive temperature probes that can be used is limited due to the pain tolerance of patients. Hence, it is important to determine the laser intensity and pattern of laser exposure in order to optimize the temperature distribution in the treated region. The determinants of temperature distributions during thermal therapy are: the power deposition pattern of the heating source, heat removal by conduction, and heat removal by blood flow forced convection. In order to determine the temperature distribution in the treated region, numerical methods must be developed to solve the bioheat transfer equation for the human body [1].

Most utilized models for the hyperthermia treatment involve the Pennes' bioheat transfer equation (BHTE). In the BHTE model, heat transfer between the blood vessels and tissue is assumed to occur mainly across the capillaries where the blood velocity is low [19]. The blood in the capillary bed instantly thermally equilibrates with the temperature of the surrounding tissue and enters the venous circulation at the local tissue temperature. Therefore, the contribution of blood flow could be modeled as a heat sink whose magnitude is proportional to the difference between the arterial supply temperature and the local tissue temperature. There are many numerical and experimental methods developed based on this model. Clegg and Roemer [2, 20] performed hyperthermia sessions on a normal canine thigh to test the ability of a state and parameter estimation method to accurately predict the complete 3D temperature distribution in experimental situations. They employed the Pennes' equation as the system model and an optimization algorithm, which is based on a least squares error objective function, used for predicting certain unknown model parameters, such as the blood perfusion and the power deposition. Martin and Bowman [14] presented the exact steady state and transient solutions for the temperature distribution in laser irradiated and perfused tissue using the Pennes' equation under cylindrical coordinates. Liauh and Roemer [11] presented a semi-linear state and parameter estimation algorithm that decreases the total computational time required to accurately reconstruct complete hyperthermia temperature fields, since the relationship between the temperature and the blood perfusion based on the Pennes' bioheat transfer equation is generally nonlinear in the hyperthermia temperature estimation problem. Chatterjee and Adams [1] generated a 2D finite element thermal model of the prostate region of the human body based on the Pennes' equation using the automatic mesh generation capabilities of the software package ANSYS.

Huang [8] considered the heat transfer within a perfused tissue in the presence of a vessel. The Pennes' bioheat transfer equation was used for the perfused tissue, and a lumped capacitance analysis was used for the convection in the vessel with a constant Nusselt number. Analytical solutions of the Pennes' bioheat transfer equation with a blood vessel were obtained. Payne [18] derived a design of the phantom from a combination of the convective fin equation and the Pennes' BHTE, and developed a phantom model using an inverse technique applied to experimental data from a thin layer phantom to determine model parameters. Majchrzak and Mochnacki [13] considered thermal processes proceeding within a perfused tissue in the presence of a vessel. The Pennes' bioheat transfer equation determines the steady state temperature field in the tissue sub-domain, while the ordinary differential equation resulting from the energy balance describes the change of blood temperature along the vessel. Dai [3–5] developed a domain decomposition method for solving the 3D Pennes' bioheat transfer equation in a triple-layered skin structure. Recently, we [31] have developed a numerical method for optimizing laser power in the irradiation of a 3D triple layered cylindrical skin structure. The method was obtained by solving numerically the 3D Pennes' bioheat equation where the surface of the skin is irradiated by the laser according to a designed pattern. From this temperature distribution, we used the least squares method in order to determine the laser intensity that gives temperatures close in value to the pre-specified temperatures to be attained at the center and perimeter of the skin surface. However, the laser exposure pattern was pre-specified in the numerical method, which makes difficulty in general to determine the laser power by minimizing the sum of squares derivations between calculated and pre-specified temperatures at center and perimeter in one step. In this article, we develop a numerical algorithm based on our previous results and taking into account both the laser intensity and laser exposure pattern, so that the numerical method can be applied to more general cases.

2. Mathematical model

In this study, we employ the Pennes' equation for obtaining the temperature distribution since it has been widely applied. It should be pointed out that our method is not limited to the Pennes' equation and could be replaced by other models. Consider a cylindrical 3D skin structure that is composed of epidermis, dermis and subcutaneous, where the surface of the skin is irradiated by a laser, as shown in Fig. 1. The Pennes' equation that describes the thermal behavior of the triple-layered skin structure when irradiated by a laser can be expressed in cylindrical coordinates as follows [19],

$$\rho_l C_l \frac{\partial T_l}{\partial t} = k_l \left[\frac{1}{r} \frac{\partial}{\partial r} (r \frac{\partial T_l}{\partial r}) + \frac{1}{r^2} \frac{\partial^2 T_l}{\partial \varphi^2} + \frac{\partial^2 T_l}{\partial z^2} \right] + W_b^l C_b^l (T_b - T_l) + Q_m^l + Q_r^l, \qquad l = 1, 2, 3, \quad (1)$$

where T_l is the tissue temperature; T_b is the artery temperature; ρ_l, C_l and k_l denote density, specific heat, and thermal conductivity of tissue, respectively; C_b^l is the specific heat of blood; W_b^l is the blood perfusion rate; and Q_m^l and Q_r^l are volumetric heats due to metabolism and spatial heating, respectively. To analyze the temperature elevation by heating, we assume T_l^m to be the steady-state temperature obtained based on the following equation,

$$0 = k_l \left[\frac{1}{r} \frac{\partial}{\partial r} \left(r \frac{\partial T_l^m}{\partial r} \right) + \frac{1}{r^2} \frac{\partial^2 T_l^m}{\partial \varphi^2} + \frac{\partial^2 T_l^m}{\partial z^2} \right] + W_b^l C_b^l (T_b - T_l^m) + Q_m^l, \qquad l = 1, 2, 3. \quad (2)$$

Let $\theta_l = T_l - T_l^m$, which is the temperature elevation above the steady-state temperature due to heating. Assume that T_b is unchanged for simplicity. Then, θ_l satisfies

$$\rho_l C_l \frac{\partial \theta_l}{\partial t} + W_b^l C_b^l \theta_l - k_l \left[\frac{1}{r} \frac{\partial}{\partial r} \left(r \frac{\partial \theta_l}{\partial r} \right) + \frac{1}{r^2} \frac{\partial^2 \theta_l}{\partial \varphi^2} + \frac{\partial^2 \theta_l}{\partial z^2} \right] = Q_r^l, \quad l = 1, 2, 3. \quad (3)$$

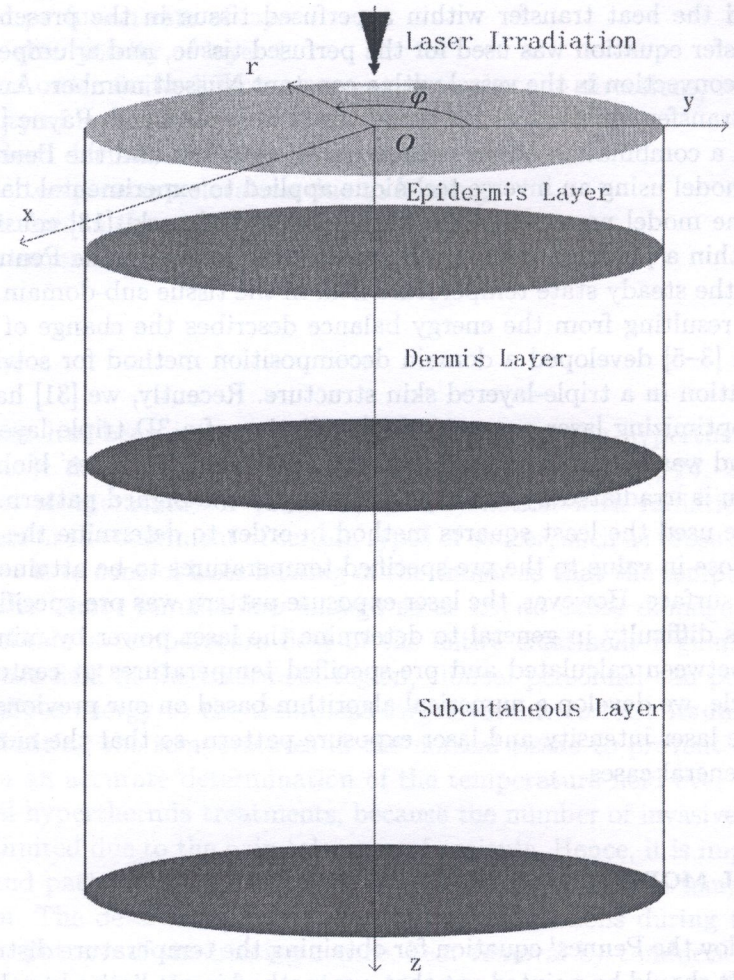

Fig. 1. Configuration of a 3D skin structure

Furthermore, we assume that the laser power is continuous and spatial with a normal distribution. As such, the heat source Q_r^l can be written as follows [9],

$$Q_1 = \alpha_1 e^{-\alpha_1 z} \frac{1}{\sqrt{2\pi\sigma^2}} e^{-\frac{(r\cos\varphi - x_0(t))^2 + (r\sin\varphi - y_0(t))^2}{2\sigma^2}} P_0(1 - Reff_1), \tag{4a}$$

$$Q_2 = \alpha_2 e^{-\alpha_1 L_1 - \alpha_2 z} \frac{1}{\sqrt{2\pi\sigma^2}} e^{-\frac{(r\cos\varphi - x_0(t))^2 + (r\sin\varphi - y_0(t))^2}{2\sigma^2}} P_0(1 - Reff_2), \tag{4b}$$

$$Q_1 = \alpha_3 e^{-\alpha_1 L_1 - \alpha_2 L_2 - \alpha_3 z} \frac{1}{\sqrt{2\pi\sigma^2}} e^{-\frac{(r\cos\varphi - x_0(t))^2 + (r\sin\varphi - y_0(t))^2}{2\sigma^2}} P_0(1 - Reff_3), \tag{4c}$$

where α_1, α_2, α_3 are laser absorptivities of the three layers, respectively; $Reff_1$, $Reff_2$, $Reff_3$ are laser reflectivities of three layers of the skin, respectively; σ is the standard deviation of the width of a normally distributed laser beam; and L_1, L_2, L_3 are depths of the three layers, respectively. Here, $(x_0(t), y_0(t))$ is the location where the laser is focused, and can vary with time t.

For simplicity, we assume that the heat flux approaches zero in the depth of the tissue, which is realistic for a biological body [12]. Further, without loss generality, we assume that the heat flux is zero at $z = 0$ in order to simplify the stability analysis. However, one may choose other boundary conditions such as heat convection on the surface. Thus, the interfacial and boundary conditions can be written as follows,

$$\frac{\partial \theta_1}{\partial z} = 0, \qquad z = 0, \tag{5}$$

$$\theta_1 = \theta_2, \quad k_1 \frac{\partial \theta_1}{\partial z} = k_2 \frac{\partial \theta_2}{\partial z}, \qquad z = L_1, \tag{6}$$

$$\theta_2 = \theta_3, \quad k_2 \frac{\partial \theta_2}{\partial z} = k_3 \frac{\partial \theta_3}{\partial z}, \qquad z = L_1 + L_2, \tag{7}$$

$$\frac{\partial \theta_3}{\partial z} = 0, \qquad z = L_1 + L_2 + L_3, \tag{8}$$

$$\frac{\partial \theta_l}{\partial r} = 0, \qquad r = R, \tag{9}$$

$$\theta_l(r, \varphi, z) = \theta_l(r, \varphi + 2m\pi, z). \tag{10}$$

The initial condition is

$$\theta_l = 0, \quad t = 0, \qquad l = 1, 2, 3. \tag{11}$$

It should be pointed put that because the location $(x_0(t), y_0(t))$ varies with time t, the unsteady-state three dimensional heat conduction equation, Eq. (3), is necessary in general.

3. Numerical method

To obtain a temperature distribution numerically, we first let $(u_l)^n_{ijk}$ be the numerical approximation of $(\theta_l)(i\Delta r, j\Delta\varphi, k\Delta z, n\Delta t)$, where Δr, $\Delta\varphi$, Δz, and Δt are the spatial and temporal mesh sizes, respectively. Here, i, j, k are chosen to be integers with $0 \le i \le N_r$, $0 \le j \le N_\varphi$, $0 \le k \le N_l^z$, so that $N_r \Delta r = R$, $N_\varphi \Delta\varphi = 2\pi$, and $N_l^z \Delta z = L_l$, $l = 1, 2, 3$. As such, a finite difference method for solving the initial and boundary triple-layered skin structure problem, Eqs. (3)–(11), can be written as follows,

$$\rho_l C_l \frac{(u_l)^{n+1}_{ijk} - (u_l)^n_{ijk}}{\Delta t} + W_b^l C_b^l \frac{(u_l)^{n+1}_{ijk} + (u_l)^n_{ijk}}{2} - k_l (P_r^2 + \delta_\varphi^2 + \delta_z^2) \frac{(u_l)^{n+1}_{ijk} + (u_l)^n_{ijk}}{2} = (Q_r^l)^{n+\frac{1}{2}}_{ijk}, \quad l = 1, 2, 3, \tag{12}$$

where

$$P_r^2 u^n_{ijk} = \frac{r_{i+\frac{1}{2}}(u^n_{i+1jk} - u^n_{ijk}) - r_{i-\frac{1}{2}}(u^n_{ijk} - u^n_{i-1jk})}{r_i \Delta r^2},$$

$$\delta_\varphi^2 u_{ijk} = \frac{u_{ij+1k} - 2u_{ijk} + u_{ij-1k}}{r_i^2 \Delta\varphi^2},$$

$$\delta_z^2 u_{ijk} = \frac{u_{ijk+1} - 2u_{ijk} + u_{ijk-1}}{\Delta z^2},$$

and $r_{i+\frac{1}{2}} = (i + \frac{1}{2})\Delta r$. The discrete interfacial equations are assumed to be, for any time level,

$$k_1 \frac{(u_1)^n_{ijN_1^z} - (u_1)^n_{ijN_1^z - 1}}{\Delta z} = k_2 \frac{(u_2)^n_{ij1} - (u_2)^n_{ij0}}{\Delta z}, \qquad (u_1)^n_{ijN_1^z} = (u_2)^n_{ij0}, \tag{13}$$

and

$$k_2 \frac{(u_2)^n_{ijN_2^z} - (u_2)^n_{ijN_2^z - 1}}{\Delta z} = k_3 \frac{(u_3)^n_{ij1} - (u_3)^n_{ij0}}{\Delta z}, \qquad (u_2)^n_{ijN_2^z} = (u_3)^n_{ij0}. \tag{14}$$

This initial and boundary conditions are discretized as follows,

$$(u_l)^0_{ijk} = 0, \tag{15}$$

$$(u_1)^n_{ij0} = (u_1)^n_{ij1}, \qquad (u_3)^n_{ijN_3^z} = (u_3)^n_{ijN_3^z-1}, \tag{16}$$

$$(u_l)^n_{N_rjk} = (u_l)^n_{N_r-1jk}, \qquad (u_l)^n_{ijk} = (u_l)^n_{ij+mN_\varphi\Delta\varphi k}, \tag{17}$$

for any time level n.

It should be pointed out that the laser intensity P_0 is unknown and will be determined by pre-specifying the temperatures to be obtained at the center and some perimeter locations on the skin surface based on the least squares method. Therefore, one needs to show that the numerical scheme, Eqs. (12)–(17), is stable with respect to P_0. We give a proof in the appendix which shows the scheme to be unconditionally stable with respect to the heat source Q_r^l (that is, P_0).

To optimize the laser intensity P_0, we pre-specify the elevated temperatures to be obtained at the center and some perimeter locations on the skin surface. The reason that the center and perimeter on the skin surface are chosen is because the temperature at these locations could be easily measured. Besides, the temperature at the perimeter of the region needs to be controlled in order to prevent damage to the tissue. By guessing an initial laser P_0, one may obtain from Eqs. (12)–(17) a temperature field in the entire 3D skin structure after the pre-specified laser exposure. Once the calculated temperatures, u^i_{cal}, at the given locations ($i = 0, 1, \ldots, M$) are obtained, a least squares approach can be employed to minimize the difference between the pre-specified elevated temperature θ_{pre} and the calculated temperature u_{cal} as follows,

$$S(P_0) = \sum_{i=0}^{M} \left[(\theta^i_{\text{pre}} - u^i_{\text{cal}})\right]^2, \qquad i = 0, 1, \ldots, M, \tag{18}$$

Minimizing $S(P_0)$ in Eq. (18), one can obtain

$$\frac{\mathrm{d}}{\mathrm{d}P_0} S(P_0) = -2 \sum_{i=0}^{M} \left(\frac{\mathrm{d}(u^i_{\text{cal}})}{\mathrm{d}P_0} \right) (\theta^i_{\text{pre}} - u^i_{\text{cal}}) = 0, \qquad i = 0, 1, \ldots, M. \tag{19}$$

Hence, a new P_0 can be calculated iteratively as follows [17],

$$P_0^{(m+1)} = P_0^{(m)} + (X^t X + \alpha^* I)^{-1} X^t (\vec{\theta}_{\text{pre}} - \vec{u}_{\text{cal}}) \tag{20}$$

where α^* is a relaxation parameter for convergence, X is the sensitivity coefficient matrix, which is a $1 \times (M+1)$ vector

$$X = \left[\frac{\partial(u^0_{\text{cal}})}{\partial P_0}, \frac{\partial(u^1_{\text{cal}})}{\partial P_0}, \ldots, \frac{\partial(u^M_{\text{cal}})}{\partial P_0} \right]^t, \tag{21}$$

and

$$\vec{\theta}_{\text{pre}} = \begin{bmatrix} \theta^0_{\text{pre}} \\ \theta^1_{\text{pre}} \\ \vdots \\ \theta^M_{\text{pre}} \end{bmatrix}, \qquad \vec{u}_{\text{cal}} = \begin{bmatrix} u^0_{\text{cal}} \\ u^1_{\text{cal}} \\ \vdots \\ u^M_{\text{cal}} \end{bmatrix}. \tag{22}$$

Hence, the required laser intensity P_0 can be obtained by guessing an initial laser intensity and its small increment, P_0 and $P_0 + \Delta P$, to obtain the temperature distributions, $\vec{u}_{\text{cal}}(P_0)$ and $\vec{u}_{\text{cal}}(P_0 + \Delta P)$, by solving Eqs. (12)–(17); determining a new P_0 by Eqs. (20)–(22), where $\frac{\partial(u_{\text{cal}})}{\partial P_0}$ is evaluated by $\frac{u_{\text{cal}}(P_0+\Delta P) - u_{\text{cal}}(P_0)}{\Delta P}$; and repeating the computation until $\frac{|S(P_0^{m+1}) - S(P_0^m)|}{S(P_0^{m+1})} < \epsilon$ is satisfied.

The algorithm for obtaining an optimal temperature distribution in a 3D triple layered cylindrical skin structure can be described as follows, as shown in Fig. 2.

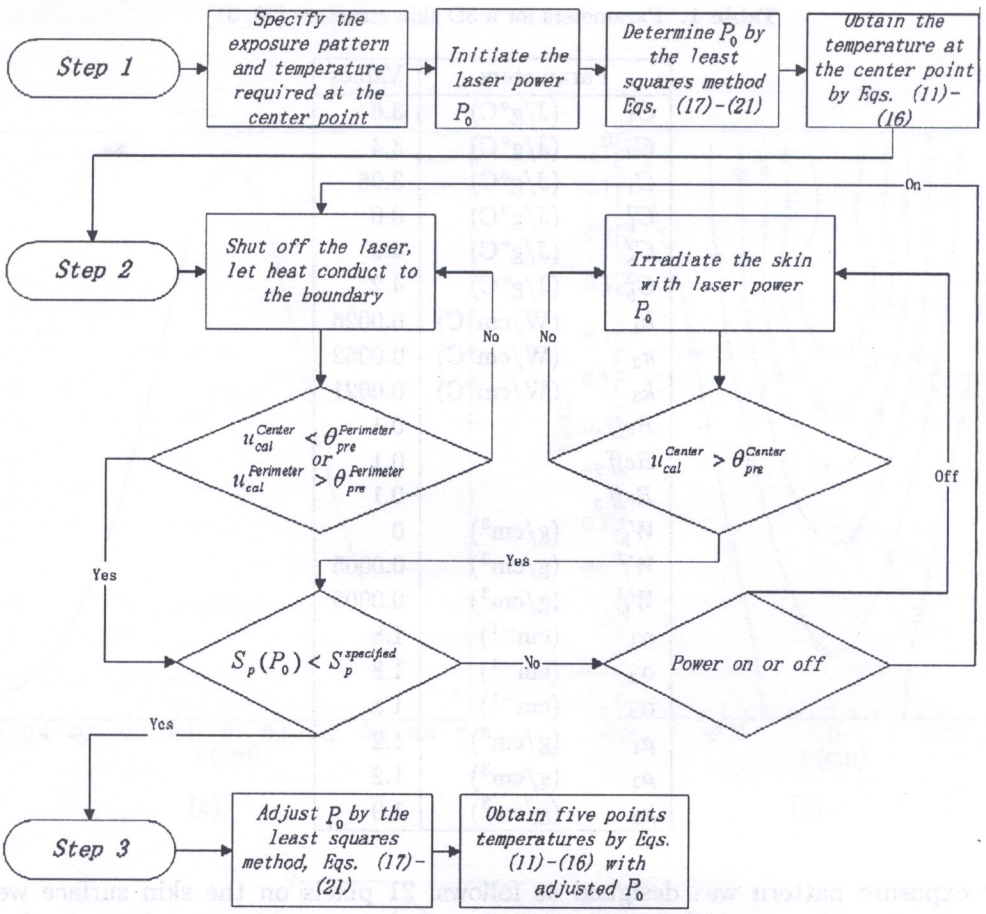

Fig. 2. Computational flow diagram of the numerical method

Step 1. Determine an initial P_0 based on the center point only so that the pre-specified temperature $\theta_{\text{pre}}^{\text{center}}$ is satisfied. This is necessary since it is difficult to determine the laser power by minimizing the sum of squares derivations between calculated (from the bioheat equation) and pre-specified temperatures at all $M+1$ points (center and perimeter) in one step.

Step 2. Turn off the laser in order to allow heat to diffuse from the center towards the perimeter of the region. This allows the perimeter temperature to increase and leads to a decrease in the temperature at the center. Based on certain criteria involving comparisons between calculated temperatures at the center ($u_{\text{cal}}^{\text{center}}$) and perimeter ($u_{\text{cal}}^{\text{perimeter}}$) and pre-specified temperature ($\theta_{\text{pre}}^{\text{center}}$, $\theta_{\text{pre}}^{\text{perimeter}}$), the laser may need to be turned on and off until $S_p(P_0) = \sum_{i=1}^{M} \left[(\theta_{\text{pre}}^{i} - u_{\text{cal}}^{i})\right]^2$ is less than a pre-specified value, $S_p^{\text{specified}}$.

Step 3. Optimize P_0 based on the least squares method, Eqs. (18)–(22), and the calculated temperature distribution, Eqs. (12)–(17), involving the $M+1$ points in Eq. (18).

4. Numerical example

We tested our algorithm in a 3D skin structure as shown in Fig. 1, where the materials were chosen from Table 1. The dimension of the skin structure was chosen to be $R = 0.5\,\text{cm}$, $L_1 = 0.008\,\text{cm}$, $L_2 = 0.02\,\text{cm}$, and $L_3 = 1.0\,\text{cm}$. A mesh of $31\times20\times1209$ in (r, φ, z) was employed in the computation. The time increment Δt is 0.1 s and the standard deviation of the laser beam width σ is 0.1. In our calculation, we pre-specified the temperature elevations at the center of the skin surface and at four locations, 90 degrees apart (that is, $\varphi = 0, \frac{\pi}{2}, \pi$, and $\frac{3\pi}{2}$), at the perimeter.

Table 1. Parameters for a 3D skin structure [28, 31]

Parameters		Values
C_1	(J/g°C)	3.6
C_2	(J/g°C)	3.4
C_1	(J/g°C)	3.06
C_b^1	(J/g°C)	0.0
C_b^2	(J/g°C)	4.2
C_b^3	(J/g°C)	4.2
k_1	(W/cm°C)	0.0026
k_2	(W/cm°C)	0.0052
k_3	(W/cm°C)	0.0021
$Reff_1$		0.1
$Reff_2$		0.1
$Reff_3$		0.1
W_b^1	(g/cm^3)	0
W_b^2	(g/cm^3)	0.0005
W_b^3	(g/cm^3)	0.0005
α_1	(cm^{-1})	1.8
α_2	(cm^{-1})	1.8
α_3	(cm^{-1})	1.8
ρ_1	(g/cm^3)	1.2
ρ_2	(g/cm^3)	1.2
ρ_3	(g/cm^3)	1.0

A laser exposure pattern was designed as follows: 21 pixels on the skin surface were chosen for laser irradiation. These included the center pixel and those grid points (20 points) with a Δr distance from the center. In step 1 of our algorithm, the laser was set to irradiate at the center pixel for 10 seconds, after which it was moved to the grid point at $\varphi = 0$ and circulated twice counter-clockwise over the 20 pixels with the laser focused for 10 seconds on each pixel. To implement this laser exposure pattern, at each pixel where the laser was focused, Eqs. (4a)–(4c) were used to determine the heat source (or heat input) for each time step, Δt, in the numerical scheme. The number of time steps of exposure at each pixel was equal to $\frac{10}{\Delta t}$. Starting at step 2, the laser was moved to the center pixel and was turned on and off as required.

In the three cases below, the temperature distribution is considered to be symmetric. Therefore, the purpose of the laser pattern in step 1 is to heat up the tissue quickly and to keep the temperature distribution as axisymmetric as possible. However, the model is general in three dimensions and can be applied to any pre-heating protocols one may choose. The three cases were tested as follows.

Case 1

The temperature elevations at the center and perimeter were pre-specified to be 8°C and 2°C, respectively. In this case, the initial P_0 was obtained to be 0.595951 (W).

Figure 3 shows the temperature elevation profiles (at $t = 410$ seconds) along the diameter of the skin surface for $\varphi = 0$ and $\varphi = \pi$, the temperature elevation contours in the cross section for $\varphi = 0$ and $\varphi = \pi$, and the temperature elevation profile along the depth (the z-direction) at the center of the skin surface. It can be seen from the figure that the temperature at the center is close to $8°C$. However, the temperature at the perimeter is below the required temperature. The relative error, $\sum_{i=0}^{4} \frac{\left[(\theta_{\text{pre}}^i - u_{\text{cal}}^i)\right]^2}{\left[\theta_{\text{pre}}^i\right]^2}$, is 0.499572. The results from Fig. 3 relate to computations in step 1 of Fig. 2.

In the following computations, the laser was turned off between $t = 410$ seconds and $t = 514$ seconds, and then turned on with a modified P_0 of 0.591449 (W) until $t = 640$ seconds.

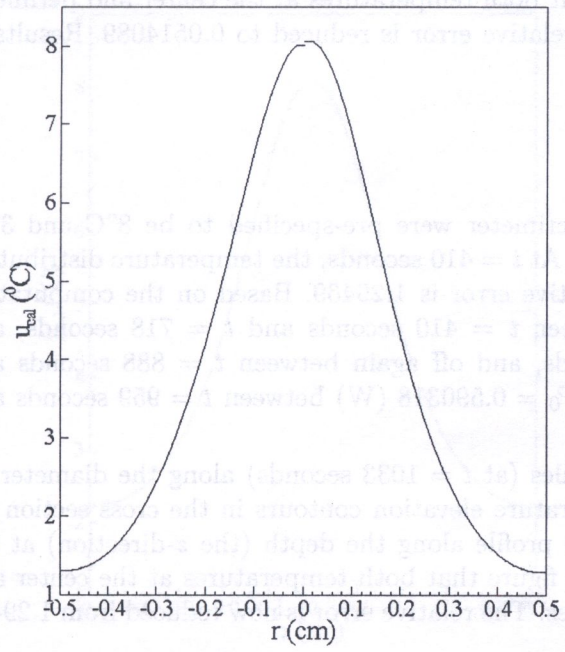

(a)

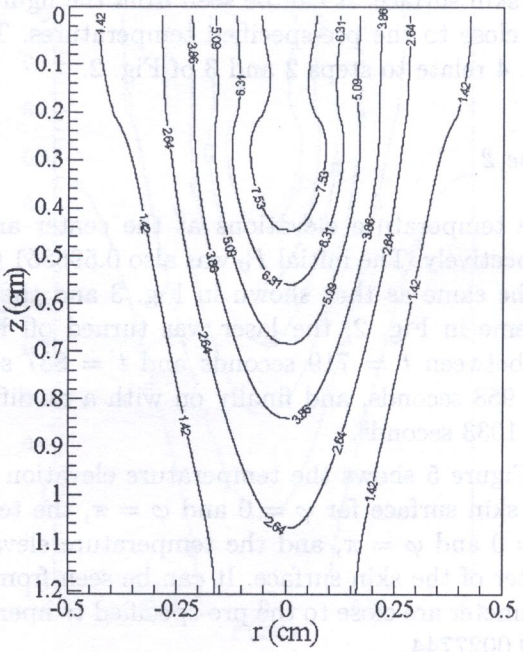

(b)

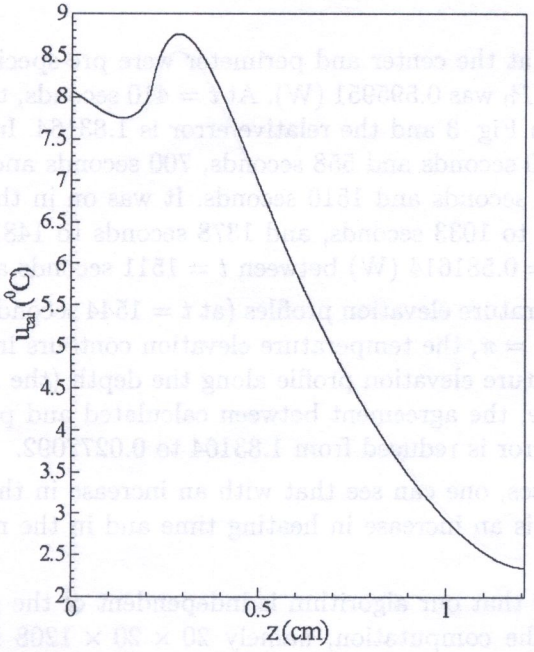

(c)

Fig. 3. (a) Temperature elevation profiles (at $t = 410$ seconds) along the diameter of the skin surface for $\varphi = 0$ and $\varphi = \pi$; (b) Temperature elevation contours in the cross section for $\varphi = 0$ and $\varphi = \pi$; (c) Temperature elevation profile along the depth (the z-direction) at the center of the skin surface

Figure 4 shows the temperature elevation profiles (at $t = 640$ seconds) along the diameter of the skin surface for $\varphi = 0$ and $\varphi = \pi$, the temperature elevation contours in the cross section for $\varphi = 0$ and $\varphi = \pi$, and the temperature elevation profile along the depth (the z-direction) at the center of the skin surface. It can be seen from the figure that both temperatures at the center and perimeter are close to the pre-specified temperatures. The relative error is reduced to 0.0514089. Results in Fig. 4 relate to steps 2 and 3 of Fig. 2.

Case 2

The temperature elevations at the center and perimeter were pre-specified to be 8°C and 3°C, respectively. The initial P_0 was also 0.595951 (W). At $t = 410$ seconds, the temperature distribution is the same as that shown in Fig. 3 and the relative error is 1.29469. Based on the computation scheme in Fig. 2, the laser was turned off between $t = 410$ seconds and $t = 718$ seconds, and on between $t = 719$ seconds and $t = 887$ seconds, and off again between $t = 888$ seconds and $t = 958$ seconds, and finally on with a modified $P_0 = 0.590318$ (W) between $t = 959$ seconds and $t = 1033$ seconds.

Figure 5 shows the temperature elevation profiles (at $t = 1033$ seconds) along the diameter on the skin surface for $\varphi = 0$ and $\varphi = \pi$, the temperature elevation contours in the cross section for $\varphi = 0$ and $\varphi = \pi$, and the temperature elevation profile along the depth (the z-direction) at the center of the skin surface. It can be seen from the figure that both temperatures at the center and perimeter are close to the pre-specified temperatures. The relative error is now reduced from 1.29469 to 0.0027744.

Case 3

The temperature elevations at the center and perimeter were pre-specified to be 8°C and 4°C, respectively. Again, the initial P_0 was 0.595951 (W). At $t = 410$ seconds, the temperature distribution is the same as that shown in Fig. 3 and the relative error is 1.83164. In this case, the laser was off in those periods between 410 seconds and 558 seconds, 700 seconds and 917 seconds, 1034 seconds and 1377 seconds, and 1482 seconds and 1510 seconds. It was on in the periods from 559 seconds to 699 seconds, 918 seconds to 1033 seconds, and 1378 seconds to 1481 seconds. Finally, the laser was on with a modified $P_0 = 0.581614$ (W) between $t = 1511$ seconds and $t = 1544$ seconds.

Figure 6 shows the temperature elevation profiles (at $t = 1544$ seconds) along the diameter of the skin surface for $\varphi = 0$ and $\varphi = \pi$, the temperature elevation contours in the cross section for $\varphi = 0$ and $\varphi = \pi$, and the temperature elevation profile along the depth (the z-direction) at the center of the skin surface. In this case, the agreement between calculated and pre-specified temperatures is improved and the relative error is reduced from 1.83164 to 0.0277092.

From the above three cases, one can see that with an increase in the pre-specified temperature elevation at the edge, there is an increase in heating time and in the number of times the laser is turned on or off.

Finally, in order to prove that our algorithm is independent of the grid size, additional meshes (r, φ, z) were employed in the computation, namely $20 \times 20 \times 1208$ in (r, φ, z), $40 \times 20 \times 1208$ in (r, φ, z) and $30 \times 20 \times 2416$ in (r, φ, z). Figure 7 shows, for the conditions in case 1, the four temperature elevation profiles (at $t = 410$ seconds) along the diameter of the skin surface obtained from the various meshes ($20 \times 20 \times 1208$, $30 \times 20 \times 1208$, $40 \times 20 \times 1208$, $30 \times 20 \times 2416$) for $\varphi = 0$ and $\varphi = \pi$ and in the z-direction. It can be seen from this figure that there are no significant differences among these solutions, implying that our scheme is grid independent.

It should be pointed out that the temperature elevation profiles and contours along the diameter of the skin surface and the cross section for $\varphi = \frac{\pi}{2}$ and $\varphi = \frac{3\pi}{2}$ were not plotted because they are virtually identical to those for $\varphi = 0$ and $\varphi = \pi$.

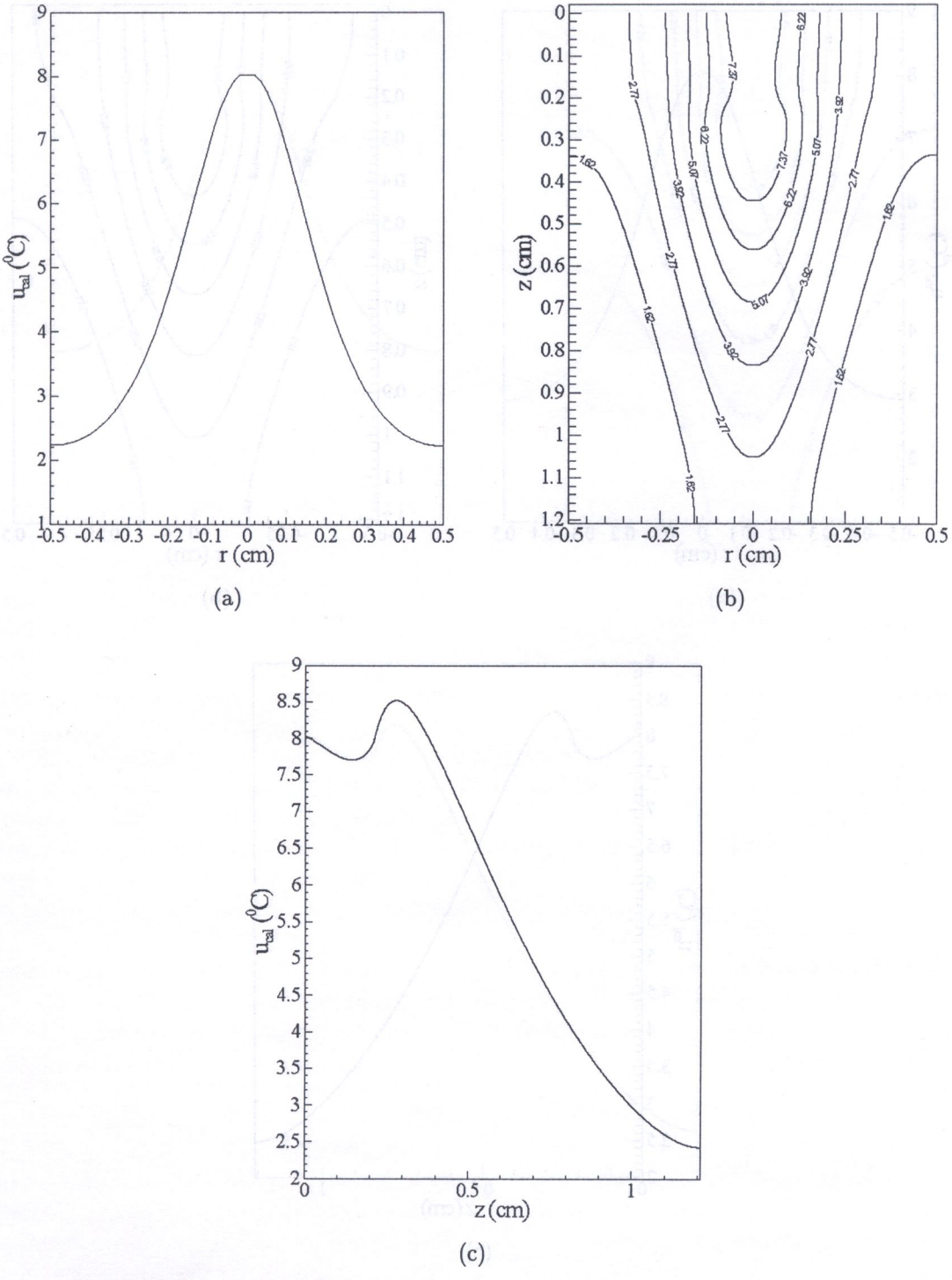

Fig. 4. (a) Temperature elevation profiles (at $t = 640$ seconds) along the diameter of the skin surface for $\varphi = 0$ and $\varphi = \pi$; (b) Temperature elevation contours in the cross section for $\varphi = 0$ and $\varphi = \pi$; (c) Temperature elevation profile along the depth (the z-direction) at the center of the skin surface

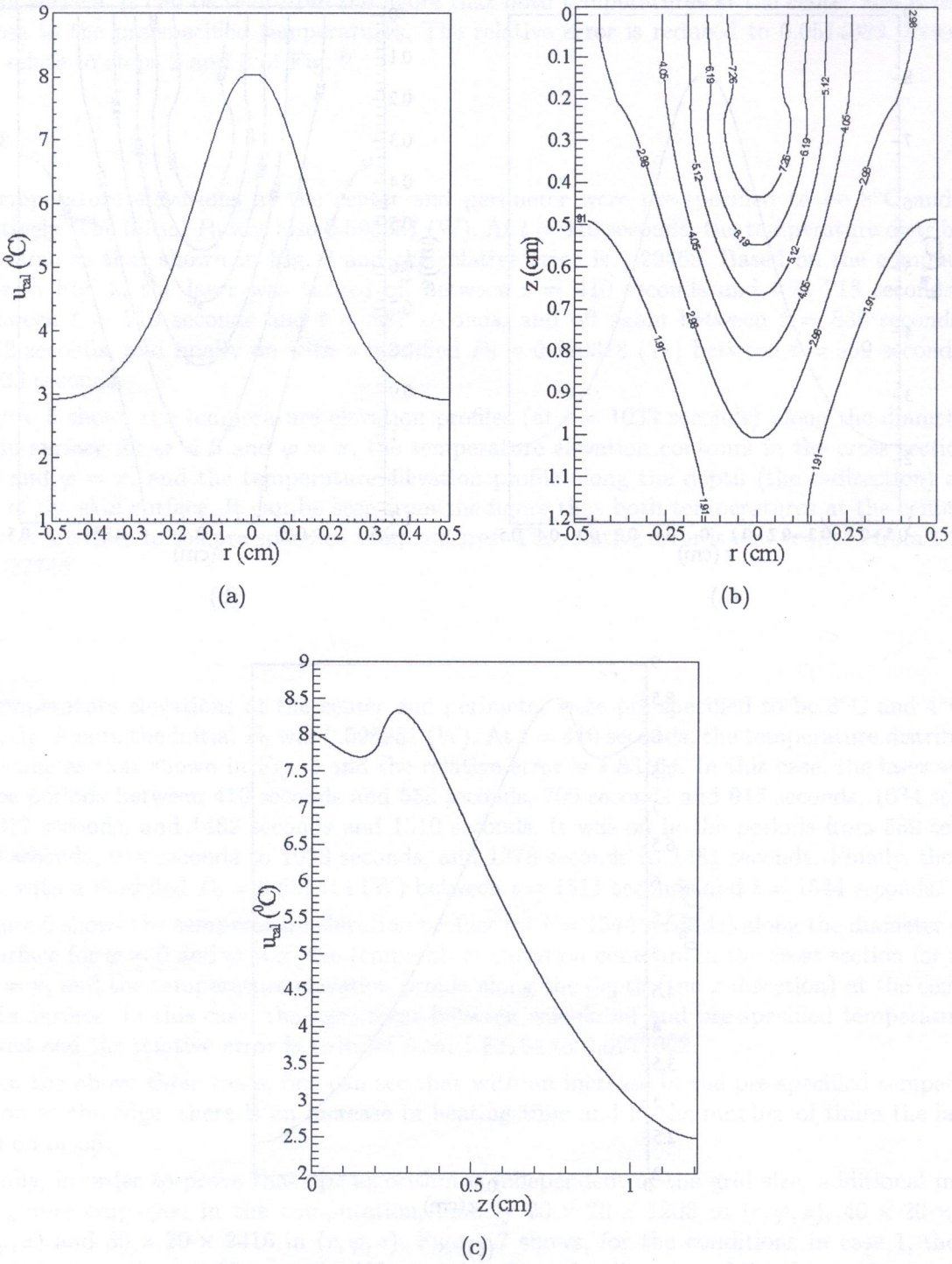

Fig. 5. (a) Temperature elevation profiles (at $t = 1033$ seconds) along the diameter of the skin surface for $\varphi = 0$ and $\varphi = \pi$; (b) Temperature elevation contours in the cross section for $\varphi = 0$ and $\varphi = \pi$; (c) Temperature elevation profile along the depth (the z-direction) at the center of the skin surface

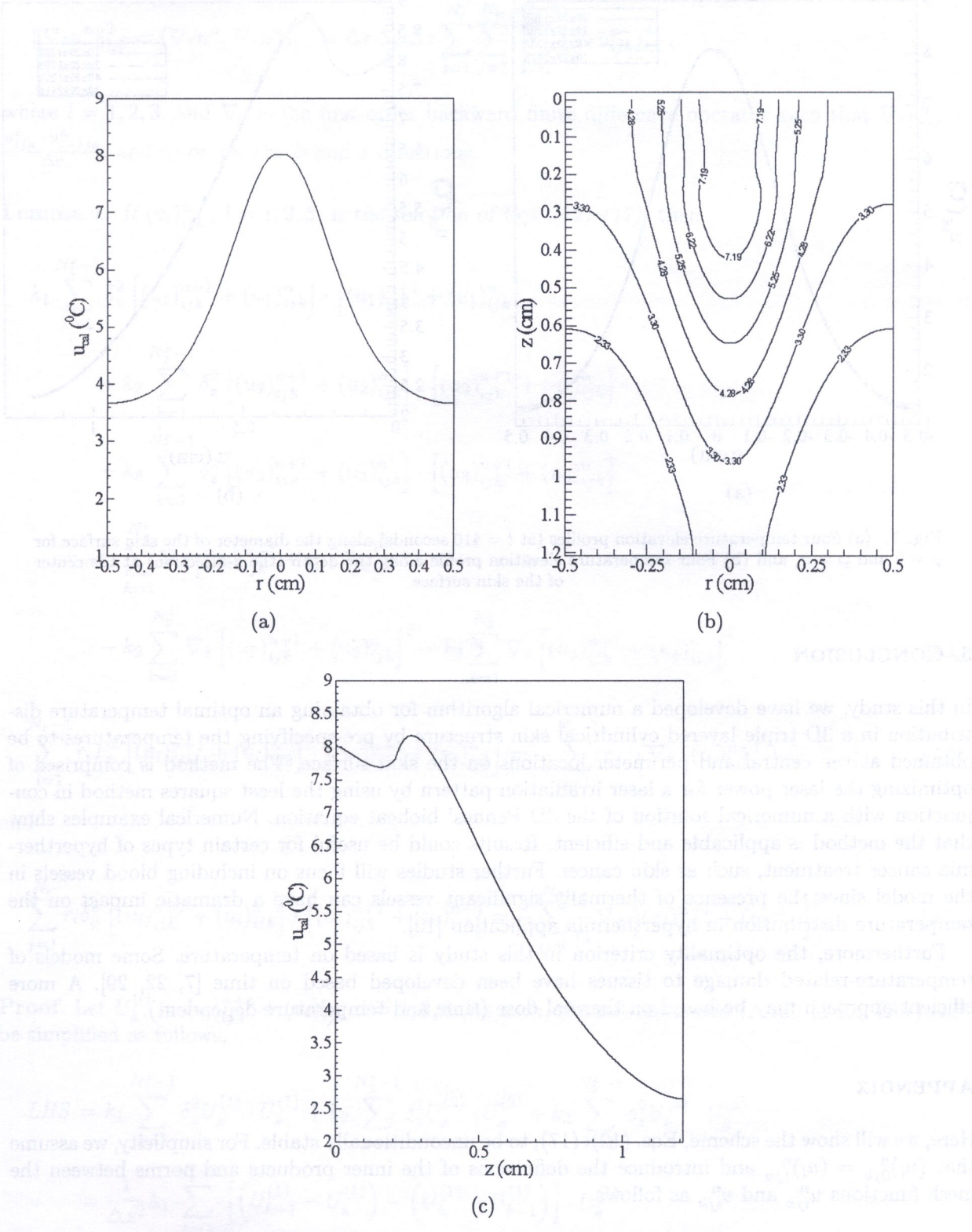

Fig. 6. (a) Temperature elevation profiles (at $t = 1544$ seconds) along the diameter of the skin surface for $\varphi = 0$ and $\varphi = \pi$; (b) Temperature elevation contours in the cross section for $\varphi = 0$ and $\varphi = \pi$; (c) Temperature elevation profile along the depth (the z-direction) at the center of the skin surface

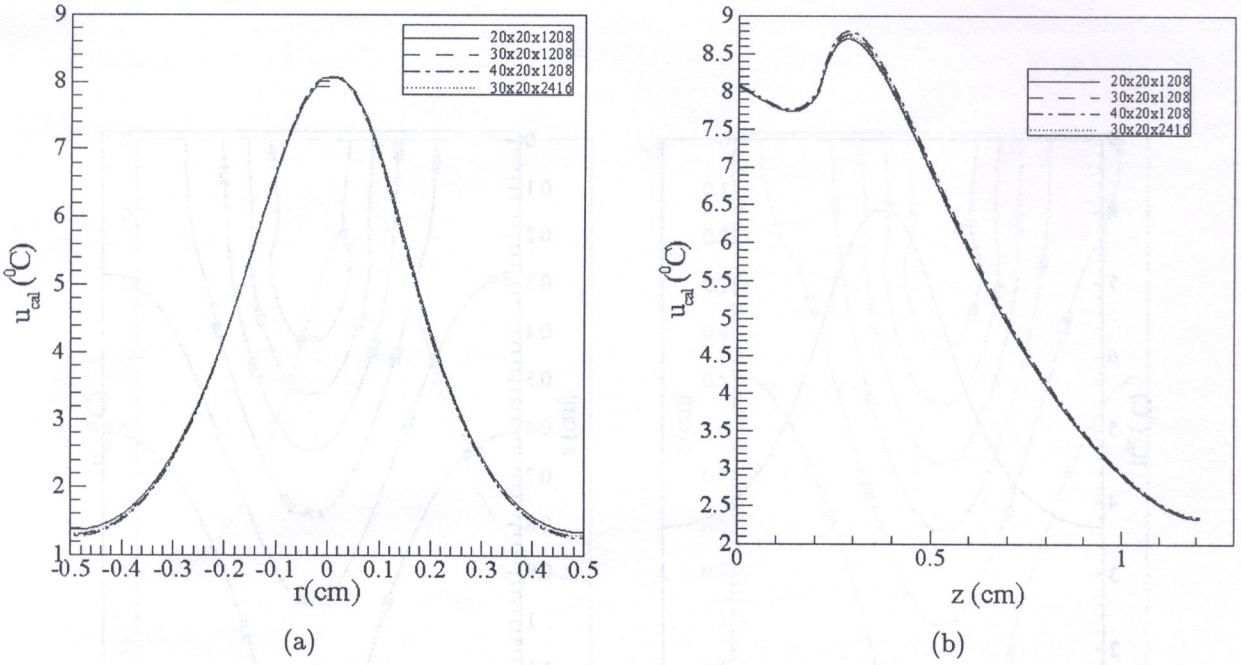

Fig. 7. (a) Four temperature elevation profiles (at $t = 410$ seconds) along the diameter of the skin surface for $\varphi = 0$ and $\varphi = \pi$, and (b) Four temperature elevation profile along the depth (the z-direction) at the center of the skin surface

5. Conclusion

In this study, we have developed a numerical algorithm for obtaining an optimal temperature distribution in a 3D triple layered cylindrical skin structure by pre-specifying the temperatures to be obtained at the central and perimeter locations on the skin surface. The method is comprised of optimizing the laser power for a laser irradiation pattern by using the least squares method in conjunction with a numerical solution of the 3D Pennes' bioheat equation. Numerical examples show that the method is applicable and efficient. Results could be useful for certain types of hyperthermia cancer treatment, such as skin cancer. Further studies will focus on including blood vessels in the model since the presence of thermally significant vessels can have a dramatic impact on the temperature distribution in hyperthermia application [10].

Furthermore, the optimality criterion in this study is based on temperature. Some models of temperature-related damage to tissues have been developed based on time [7, 22, 29]. A more efficient approach may be based on thermal dose (time and temperature-dependent).

Appendix

Here, we will show the scheme, Eqs. (12)–(17), to be unconditionally stable. For simplicity, we assume that $(u_l)^n_{0jk} = (u_l)^n_{1jk}$ and introduce the definitions of the inner products and norms between the mesh functions u^n_{ijk} and v^n_{ijk} as follows,

$$(u^n, v^n)_l = \Delta r \Delta\varphi \Delta z \sum_{i=1}^{N_r-1} \sum_{j=1}^{N_\varphi} \sum_{k=1}^{N_l^z-1} u^n_{ijk} v^n_{ijk}, \qquad \|u^n\|_l^2 = (u^n, u^n)_l ,$$

$$\|\nabla_{\bar{r}} u^n\|_l^2 = (\nabla_{\bar{r}} u^n, \nabla_{\bar{r}} u^n)_l = \Delta r \Delta\varphi \Delta z \sum_{i=1}^{N_r-1} \sum_{j=1}^{N_\varphi} \sum_{k=1}^{N_l^z-1} (\nabla_{\bar{r}} u^n_{ijk})_l^2 ,$$

$$\|\nabla_{\bar{r}} u^n\|_{l,1}^2 = (\nabla_{\bar{r}} u^n, \nabla_{\bar{r}} u^n)_{l,1} = \Delta r \Delta\varphi \Delta z \sum_{i=1}^{N_r} \sum_{j=1}^{N_\varphi} \sum_{k=1}^{N_l^z - 1} (\nabla_{\bar{r}} u_{ijk}^n)_{l,1}^2 ,$$

where $l = 1, 2, 3$, and $\nabla_{\bar{r}}$ is the first-order backward finite difference operator such that $\nabla_{\bar{r}} u_{ijk}^n = \frac{u_{ijk}^n - u_{i-1jk}^n}{\Delta r}$, and so on for the φ and z directions.

Lemma 1. *If* $(u_l)_{ijk}^n$, $l = 1, 2, 3$, *is the solution of Eqs. (12)–(17), then*

$$\begin{aligned}
&k_1 \sum_{k=1}^{N_1^z - 1} \delta_z^2 \left[(u_1)_{ijk}^{n+1} + (u_1)_{ijk}^n\right] \cdot \left[(u_1)_{ijk}^{n+1} + (u_1)_{ijk}^n\right] \\
&\quad + k_2 \sum_{k=1}^{N_2^z - 1} \delta_z^2 \left[(u_2)_{ijk}^{n+1} + (u_2)_{ijk}^n\right] \cdot \left[(u_2)_{ijk}^{n+1} + (u_2)_{ijk}^n\right] \\
&\quad + k_3 \sum_{k=1}^{N_3^z - 1} \delta_z^2 \left[(u_3)_{ijk}^{n+1} + (u_3)_{ijk}^n\right] \cdot \left[(u_3)_{ijk}^{n+1} + (u_3)_{ijk}^n\right] \\
&= -k_1 \sum_{k=1}^{N_1^z} \nabla_{\bar{z}} \left[(u_1)_{ijk}^{n+1} + (u_1)_{ijk}^n\right]^2 \\
&\quad - k_2 \sum_{k=1}^{N_2^z} \nabla_{\bar{z}} \left[(u_2)_{ijk}^{n+1} + (u_2)_{ijk}^n\right]^2 - k_3 \sum_{k=1}^{N_3^z} \nabla_{\bar{z}} \left[(u_3)_{ijk}^{n+1} + (u_3)_{ijk}^n\right]^2 ,
\end{aligned} \tag{A1}$$

$$\sum_{i=1}^{N_r - 1} r_i P_r^2 \left[(u_l)_{ijk}^{n+1} + (u_l)_{ijk}^n\right] \cdot \left[(u_l)_{ijk}^{n+1} + (u_l)_{ijk}^n\right] = - \sum_{i=1}^{N_r - 1} r_{i-\frac{1}{2}} \nabla_{\bar{r}} \left[(u_l)_{ijk}^{n+1} + (u_l)_{ijk}^n\right]^2 , \tag{A2}$$

and

$$\sum_{j=1}^{N_r} r_i \delta_\varphi^2 \left[(u_l)_{ijk}^{n+1} + (u_l)_{ijk}^n\right] \cdot \left[(u_l)_{ijk}^{n+1} + (u_l)_{ijk}^n\right] = - \sum_{j=1}^{N_r} \frac{1}{r_i} \nabla_{\bar{\varphi}} \left[(u_l)_{ijk}^{n+1} + (u_l)_{ijk}^n\right]^2 . \tag{A3}$$

Proof. Let $U_k^{(l)} = (u_l)_{ijk}^{n+1} + (u_l)_{ijk}^n$, $l = 1, 2, 3$. As such, the left-hand-side (LHS) of Eq. (A1) can be simplified as follows,

$$\begin{aligned}
LHS &= k_1 \sum_{k=1}^{N_1^z - 1} \delta_z^2 U_k^{(1)} \cdot U_k^{(1)} + k_2 \sum_{k=1}^{N_2^z - 1} \delta_z^2 U_k^{(2)} \cdot U_k^{(2)} + k_3 \sum_{k=1}^{N_3^z - 1} \delta_z^2 U_k^{(3)} \cdot U_k^{(3)} \\
&= \frac{1}{\Delta z^2} k_1 \sum_{k=1}^{N_1^z - 1} \left[\left(U_{k+1}^{(1)} - U_k^{(1)}\right) - \left(U_k^{(1)} - U_{k-1}^{(1)}\right)\right] \cdot U_k^{(1)} \\
&\quad + \frac{1}{\Delta z^2} k_2 \sum_{k=1}^{N_2^z - 1} \left[\left(U_{k+1}^{(2)} - U_k^{(2)}\right) - \left(U_k^{(2)} - U_{k-1}^{(2)}\right)\right] \cdot U_k^{(2)} \\
&\quad + \frac{1}{\Delta z^2} k_3 \sum_{k=1}^{N_3^z - 1} \left[\left(U_{k+1}^{(3)} - U_k^{(3)}\right) - \left(U_k^{(3)} - U_{k-1}^{(3)}\right)\right] \cdot U_k^{(3)}
\end{aligned}$$

$$= \frac{1}{\Delta z^2} k_1 \left[\sum_{k=2}^{N_1^z} \left(U_k^{(1)} - U_{k-1}^{(1)} \right) \cdot U_{k-1}^{(1)} - \sum_{k=1}^{N_1^z - 1} \left(U_k^{(1)} - U_{k-1}^{(1)} \right) \cdot U_k^{(1)} \right]$$

$$+ \frac{1}{\Delta z^2} k_2 \left[\sum_{k=2}^{N_2^z} \left(U_k^{(2)} - U_{k-1}^{(2)} \right) \cdot U_{k-1}^{(2)} - \sum_{k=1}^{N_2^z - 1} \left(U_k^{(2)} - U_{k-1}^{(2)} \right) \cdot U_k^{(2)} \right]$$

$$+ \frac{1}{\Delta z^2} k_3 \left[\sum_{k=2}^{N_3^z} \left(U_k^{(3)} - U_{k-1}^{(3)} \right) \cdot U_{k-1}^{(3)} - \sum_{k=1}^{N_3^z - 1} \left(U_k^{(3)} - U_{k-1}^{(3)} \right) \cdot U_k^{(3)} \right]. \tag{A4}$$

Based on Eq. (16), the *LHS* can be further written as follows,

$$LHS = \frac{1}{\Delta z^2} k_1 \left[\sum_{k=1}^{N_1^z - 1} \left(U_k^{(1)} - U_{k-1}^{(1)} \right) \cdot U_{k-1}^{(1)} - \sum_{k=1}^{N_1^z - 1} \left(U_k^{(1)} - U_{k-1}^{(1)} \right) \cdot U_k^{(1)} \right]$$

$$+ \frac{1}{\Delta z^2} k_2 \left[\sum_{k=1}^{N_2^z - 1} \left(U_k^{(2)} - U_{k-1}^{(2)} \right) \cdot U_{k-1}^{(2)} - \sum_{k=1}^{N_2^z - 1} \left(U_k^{(2)} - U_{k-1}^{(2)} \right) \cdot U_k^{(2)} \right]$$

$$+ \frac{1}{\Delta z^2} k_3 \left[\sum_{k=1}^{N_3^z - 1} \left(U_k^{(3)} - U_{k-1}^{(3)} \right) \cdot U_{k-1}^{(3)} - \sum_{k=1}^{N_3^z - 1} \left(U_k^{(3)} - U_{k-1}^{(3)} \right) \cdot U_k^{(3)} \right]$$

$$+ \frac{1}{\Delta z^2} k_1 \left(U_{N_1^z}^{(1)} - U_{N_1^z - 1}^{(1)} \right) \cdot U_{N_1^z - 1}^{(1)} - \frac{1}{\Delta z^2} k_2 \left(U_1^{(2)} - U_0^{(2)} \right) \cdot U_0^{(2)}$$

$$+ \frac{1}{\Delta z^2} k_2 \left(U_{N_2^z}^{(2)} - U_{N_2^z - 1}^{(2)} \right) \cdot U_{N_2^z - 1}^{(2)} - \frac{1}{\Delta z^2} k_3 \left(U_1^{(3)} - U_0^{(3)} \right) \cdot U_0^{(3)}.$$

Using Eqs. (11)–(12) and then Eq. (14), we simplify the above *LHS* as follows,

$$LHS = -k_1 \sum_{k=1}^{N_1^z - 1} \nabla_{\bar{z}} U_k^{(1)} \cdot \nabla_{\bar{z}} U_k^{(1)} - k_2 \sum_{k=1}^{N_2^z - 1} \nabla_{\bar{z}} U_k^{(2)} \cdot \nabla_{\bar{z}} U_k^{(2)} - k_3 \sum_{k=1}^{N_3^z - 1} \nabla_{\bar{z}} U_k^{(3)} \cdot \nabla_{\bar{z}} U_k^{(3)}$$

$$+ \frac{1}{\Delta z^2} k_1 \left(U_{N_1^z}^{(1)} - U_{N_1^z - 1}^{(1)} \right) \cdot U_{N_1^z - 1}^{(1)} - \frac{1}{\Delta z^2} k_1 \left(U_{N_1^z}^{(1)} - U_{N_1^z - 1}^{(1)} \right) \cdot U_{N_1^z}^{(1)}$$

$$+ \frac{1}{\Delta z^2} k_2 \left(U_{N_2^z}^{(2)} - U_{N_2^z - 1}^{(2)} \right) \cdot U_{N_2^z - 1}^{(2)} - \frac{1}{\Delta z^2} k_2 \left(U_{N_2^z}^{(2)} - U_{N_2^z - 1}^{(2)} \right) \cdot U_{N_2^z}^{(2)}$$

$$= -k_1 \sum_{k=1}^{N_1^z} \nabla_{\bar{z}} U_k^{(1)} \cdot \nabla_{\bar{z}} U_k^{(1)} - k_2 \sum_{k=1}^{N_2^z} \nabla_{\bar{z}} U_k^{(2)} \cdot \nabla_{\bar{z}} U_k^{(2)} - k_3 \sum_{k=1}^{N_3^z} \nabla_{\bar{z}} U_k^{(3)} \cdot \nabla_{\bar{z}} U_k^{(3)}, \tag{A5}$$

which is the right-hand-side of Eq. (A1). Using a similar argument, one may obtain Eqs. (A2) and (A3).

To show the scheme to be unconditionally stable with respect to the heat source, we assume that solutions $(u_l)_{ijk}^n$ and $(v_l)_{ijk}^n$, $l = 1, 2, 3$, are obtained by the scheme, Eq. (12), with the same initial, boundary and interfacial conditions, Eqs. (13)–(17), except different source terms, $(Q_1)_r^l$ and $(Q_2)_r^l$. We let $(\varepsilon_l)_{ijk}^n = (u_l)_{ijk}^n - (v_l)_{ijk}^n$ and $\sigma_l = (Q_1)_r^l - (Q_2)_r^l$. One may see that $(\varepsilon_l)_{ijk}^n$ satisfies Eqs. (13)–(17) and the following equation,

$$\rho_l C_l \frac{(\varepsilon_l)_{ijk}^{n+1} - (\varepsilon_l)_{ijk}^n}{\Delta t} + W_b^l C_b^l \frac{(\varepsilon_l)_{ijk}^{n+1} + (\varepsilon_l)_{ijk}^n}{2} - k_l (P_r^2 + \delta_\varphi^2 + \delta_z^2) \frac{(\varepsilon_l)_{ijk}^{n+1} + (\varepsilon_l)_{ijk}^n}{2} = (\sigma_l)_{ijk}^{n+\frac{1}{2}},$$
$$l = 1, 2, 3. \tag{A6}$$

Multiplying Eq. (A6) with $l = 1$ by $2r_i\Delta r\Delta\varphi\Delta z\Delta t[(\varepsilon_1)_{ijk}^{n+1} + (\varepsilon_1)_{ijk}^n]$, Eq. (A6) with $l = 2$ by $2r_i\Delta r\Delta\varphi\Delta z\Delta t[(\varepsilon_2)_{ijk}^{n+1} + (\varepsilon_2)_{ijk}^n]$, and Eq. (A6) with $l = 3$ by $2r_i\Delta r\Delta\varphi\Delta z\Delta t[(\varepsilon_3)_{ijk}^{n+1} + (\varepsilon_3)_{ijk}^n]$, summing over i, j, k from $1 \le i \le N_r - 1$, $1 \le j \le N_\varphi$, $1 \le k \le N_l^z - 1$, respectively, adding them together and then using Lemma 1, one obtains

$$\begin{aligned}
&\sum_{l=1}^{3} 2\rho_l C_l \left[\left\| \sqrt{r}(\varepsilon_l)^{n+1} \right\|^2 - \left\| \sqrt{r}(\varepsilon_l)^n \right\|^2 \right] + \Delta t \sum_{l=1}^{3} W_b^l C_b^l \left\| \sqrt{r} \left[(\varepsilon_l)^{n+1} + (\varepsilon_l)^n \right] \right\|^2 \\
&\quad + \Delta t \sum_{l=1}^{3} k_l \left\| \sqrt{E^{-\frac{1}{2}} r} \left[\nabla_{\bar{r}} (\varepsilon_l)^{n+1} + \nabla_{\bar{r}} (\varepsilon_l)^n \right] \right\|_l^2 \\
&\quad + \Delta t \sum_{l=1}^{3} k_l \left\| \sqrt{\frac{1}{r}} \left[\nabla_{\bar{\varphi}} (\varepsilon_l)^{n+1} + \nabla_{\bar{\varphi}} (\varepsilon_l)^n \right] \right\|_l^2 + \Delta t \sum_{l=1}^{3} k_l \left\| \sqrt{r} \left[\nabla_{\bar{z}} (\varepsilon_l)^{n+1} + \nabla_{\bar{z}} (\varepsilon_l)^n \right] \right\|_{l,1}^2 \\
&= 2\Delta t \sum_{l=1}^{3} \left((\sigma_l)^{n+\frac{1}{2}}, r \left[(\varepsilon_l)^{n+1} + (\varepsilon_l)^n \right] \right), \qquad \text{(A7)}
\end{aligned}$$

where $E^{-\frac{1}{2}}$ is a shift operator such that $E^{-\frac{1}{2}} r_i = r_{i-\frac{1}{2}}$. By the generalized Cauchy–Schwarz's inequality, we have

$$\begin{aligned}
2\left((\sigma_l)^{n+\frac{1}{2}}, r \left[(\varepsilon_l)^{n+1} + (\varepsilon_l)^n \right] \right) &\le \epsilon \left\| \sqrt{r} \left[(\varepsilon_l)^{n+1} + (\varepsilon_l)^n \right] \right\|_1^2 + \epsilon^{-1} \left\| \sqrt{r} (\sigma_l)^{n+\frac{1}{2}} \right\|^2 \\
&\le 2\epsilon \left\| \sqrt{r} (\varepsilon_l)^{n+1} \right\|^2 + 2\epsilon \left\| \sqrt{r} (\varepsilon_l)^n \right\|^2 + \epsilon^{-1} \left\| \sqrt{r} (\sigma_l)^{n+\frac{1}{2}} \right\|^2, \qquad \text{(A8)}
\end{aligned}$$

where ϵ is a positive constant. Substituting Eq. (A8) into Eq. (A7), we obtain

$$\begin{aligned}
&\sum_{l=1}^{3} (2\rho_l C_l - 2\epsilon\Delta t) \left\| \sqrt{r} (\varepsilon_l)^{n+1} \right\|^2 + \Delta t \sum_{l=1}^{3} W_b^l C_b^l \left\| \sqrt{r} \left[(\varepsilon_l)^{n+1} + (\varepsilon_l)^n \right] \right\|^2 \\
&\quad + \Delta t \sum_{l=1}^{3} k_l \left\| \sqrt{E^{-\frac{1}{2}} r} \left[\nabla_{\bar{r}} (\varepsilon_l)^{n+1} + \nabla_{\bar{r}} (\varepsilon_l)^n \right] \right\|_l^2 \\
&\quad + \Delta t \sum_{l=1}^{3} k_l \left\| \sqrt{\frac{1}{r}} \left[\nabla_{\bar{\varphi}} (\varepsilon_l)^{n+1} + \nabla_{\bar{\varphi}} (\varepsilon_l)^n \right] \right\|_l^2 + \Delta t \sum_{l=1}^{3} k_l \left\| \sqrt{r} \left[\nabla_{\bar{z}} (\varepsilon_l)^{n+1} + \nabla_{\bar{z}} (\varepsilon_l)^n \right] \right\|_{l,1}^2 \\
&\le \sum_{l=1}^{3} (2\rho_l C_l + 2\epsilon\Delta t) \left\| \sqrt{r} (\varepsilon_l)^n \right\|^2 + \Delta t \sum_{l=1}^{3} \epsilon^{-1} \left\| \sqrt{r} (\sigma_l)^{n+\frac{1}{2}} \right\|^2. \qquad \text{(A9)}
\end{aligned}$$

We denote $F(n) = \sum_{l=1}^{3} 2\rho_l C_l \left\| \sqrt{r} (\varepsilon_l)^n \right\|^2$. Choosing $\epsilon = \rho_l C_l$, taking out the second, third, fourth, and fifth terms on the left hand side of Eq. (A9), we simplify Eq. (A9) as follows,

$$(1 - \Delta t) F(n+1) \le (1 + \Delta t) F(n) + \Delta t \sum_{l=1}^{3} \frac{1}{\rho_l C_l} \left\| \sqrt{r} (\sigma_l)^{n+\frac{1}{2}} \right\|^2. \qquad \text{(A10)}$$

Thus, we obtain

$$
\begin{aligned}
F(n+1) &\le \frac{1+\Delta t}{1-\Delta t}F(n) + \frac{\Delta t}{1-\Delta t}\sum_{l=1}^{3}\frac{1}{\rho_l C_l}\left\|\sqrt{r}(\sigma_l)^{n+\frac{1}{2}}\right\|^2 \\
&\le \frac{(1+\Delta t)}{(1-\Delta t)}\left[\frac{(1+\Delta t)}{(1-\Delta t)}F(n-1) + \frac{\Delta t}{1-\Delta t}\sum_{l=1}^{3}\frac{1}{\rho_l C_l}\left\|\sqrt{r}(\sigma_l)^{n-\frac{1}{2}}\right\|^2\right] \\
&\quad + \frac{\Delta t}{1-\Delta t}\sum_{l=1}^{3}\frac{1}{\rho_l C_l}\left\|\sqrt{r}(\sigma_l)^{n+\frac{1}{2}}\right\|^2 \\
&\le \cdots \\
&\le \left(\frac{1+\Delta t}{1-\Delta t}\right)^{n+1}F(0) + \frac{\Delta t}{1-\Delta t}\left[1+\frac{1+\Delta t}{1-\Delta t}+\cdots+\left(\frac{1+\Delta t}{1-\Delta t}\right)^{n}\right] \\
&\qquad \cdot\sum_{l=1}^{3}\frac{1}{\rho_l C_l}\max_{0\le m\le n}\left\|\sqrt{r}(\sigma_l)^{m+\frac{1}{2}}\right\|^2 \\
&\le \left(\frac{1+\Delta t}{1-\Delta t}\right)^{n+1}F(0) + \frac{\Delta t}{(1-\Delta t)}\left[\frac{1-\left(\frac{1+\Delta t}{1-\Delta t}\right)^{n+1}}{1-\left(\frac{1+\Delta t}{1-\Delta t}\right)}\right]\sum_{l=1}^{3}\frac{1}{\rho_l C_l}\max_{0\le m\le n}\left\|\sqrt{r}(\sigma_l)^{m+\frac{1}{2}}\right\|^2 \\
&\le \left(\frac{1+\Delta t}{1-\Delta t}\right)^{n+1}\left[F(0)+\sum_{l=1}^{3}\frac{1}{\rho_l C_l}\max_{0\le m\le n}\left\|\sqrt{r}(\sigma_l)^{m+\frac{1}{2}}\right\|^2\right]. \qquad \text{(A11)}
\end{aligned}
$$

Using the inequalities $(1+\epsilon)^n \le e^{n\epsilon}$ for $\epsilon > 0$, and $(1-\epsilon)^{-1} \le e^{2\epsilon}$ when $0 < \epsilon \le \frac{1}{2}$, we obtain

$$
F(n+1) \le e^{3(n+1)\Delta t}\left[F(0)+\sum_{l=1}^{3}\frac{1}{\rho_l C_l}\max_{0\le m\le n}\left\|\sqrt{r}(\sigma_l)^{m+\frac{1}{2}}\right\|^2\right], \qquad \text{(A12)}
$$

when $\Delta t \le \frac{1}{2}$. From Eq. (A12), we obtain that $F(0) = 0$ and hence

$$
F(n+1) \le e^{3t_0}\sum_{l=1}^{3}\frac{1}{\rho_l C_l}\max_{0\le m\le n}\left\|\sqrt{r}(\sigma_l)^{m+\frac{1}{2}}\right\|^2, \qquad \text{(A13)}
$$

for $0 \le (n+1)\Delta t \le t_0$. The following theorem has then been obtained:

Theorem 1. *Assume that solutions $(u_l)_{ijk}^n$ and $(v_l)_{ijk}^n$, $l = 1, 2, 3$, are obtained by the scheme, Eq. (12), with the same initial, boundary and interfacial conditions, Eqs. (13)–(17), except different source terms, $(Q_1)_r^l$ and $(Q_2)_r^l$. Let $(\varepsilon_l)_{ijk}^n = (u_l)_{ijk}^n - (v_l)_{ijk}^n$ and $\sigma_l = (Q_1)_r^l - (Q_2)_r^l$. Then $(\varepsilon_l)_{ijk}^n$ satisfies, for $0 \le n\Delta t \le t_0$,*

$$
\sum_{l=1}^{3} 2\rho_l C_l\left\|\sqrt{r}(\varepsilon_l)^n\right\|^2 \le e^{3t_0}\sum_{l=1}^{3}\frac{1}{\rho_l C_l}\max_{0\le m\le n-1}\left\|\sqrt{r}(\sigma_l)^{m+\frac{1}{2}}\right\|^2, \qquad \text{(A14)}
$$

which implies that the scheme is unconditionally stable with respect to the heat source.

References

[1] I. Chatterjee, R.A. Adams. Finite element thermal modelling of the human body under hyperthermia treatment for cancer. *Int. J. of Computer Applications in Technology*, **7**: 151–159, 1994.

[2] S.T. Clegg, R.B. Roemer. Predictions of three-dimensional temperature distributions during hyperthermia experiments. *ASME Heat Transfer Division*, **126**: 29–35, 1989.

[3] W. Dai, G. Li, R. Nassar, T. Zhu. A domain decomposition method for solving the Pennes' bioheat transfer in a 3D triple-layered skin structure. *Proceedings of the Second M.I.T. Conference on Computational Fluid and Solid Mechanics*, MIT, Boston, **2**: 1650–1659, June 17-20, 2003.

[4] W. Dai, H. Yu, R. Nassar, T. Zhu. A fourth-order compact finite difference scheme for solving a 1-D Pennes' bioheat transfer equation in a uniform tissue. *Proceedings of the 2003 International Conference on Mathematics and Engineering Techniques in Medicine and Biological Sciences*, Las Vegas, Nevada, 336-339, June 23–26, 2003.

[5] W. Dai, H. Yu, R. Nassar. A fourth-order compact finite difference scheme for solving a 1-D Pennes' bioheat transfer equation in a triple-layered skin structure. *Numerical Heat Transfer*, **46**: 447–461, 2004.

[6] E.J. Hall, L. Roizin-Towle. Biological effects of heat. *Cancer Res.*, **44**: 4708s–4713s, 1984.

[7] F.C. Henriquez Jr. Studies of thermal injury: V. The predictability and the significance of thermally induced rate processes leading to irreversible epidermal injury. *Arch. Pathology*, **43**: 489–502, 1947.

[8] H.W. Huang, C.L. Chan, R.B. Roemer. Analytical solutions of Pennes bioheat transfer equation with a blood vessel. *Journal of Biomechanical Engineering*, **116**: 208–212, 1994.

[9] H. Jaesung, F.J. Klavs. Combined experimental and modeling studies of laser-assisted chemical vapor deposition of copper from copper (I)-hexafluoroacetylacetonate trimethylvinylsilane. *J. Appl. Phys.*, **75**: 2240–2250, 1994.

[10] S.G. Klemick, M.A. Jog, P.S. Ayyaswamy. Numerical evaluation of heat clearance properties of a radiatively heated biological tissue by adaptive grid scheme. *Numerical Heat Transfer, Part A*, **31**: 451–467, 1997.

[11] C.T. Liauh, R.B. Roemer. A semilinear state and parameter estimation algorithm for inverse hyperthermia problems. *Journal of Biomechanical Engineering*, **115**: 257–261, 1993.

[12] J. Liu, X. Chen, L.X. Xu. New thermal wave aspects on burn evaluation of skin subjected to instantaneous heating. *IEEE Transaction on Biomedical Engineering*, **46**: 420–428, 1999.

[13] E. Majchrzak, B. Mochnacki. Numerical model of heat transfer between blood vessel and biological tissue. *Computer Assisted Mechanics and Engineering Sciences*, **6**: 439–447, 1999.

[14] G.T. Martin, H.F. Bowman. The temperature distribution in laser irradiated tissue with blood perfusion. *ASME Heat Transfer Division*, **126**: 97–102, 1989.

[15] P. Moroz, S.K. Jones, B.N. Gary. Magnetically mediated hyperthermia: Current status and future directions. *Int. J. Hyperthermia*, **18**: 267–284, 2002.

[16] V. Muralidharan, C. Malcontenti-Wilson, C. Cristophi. Interstitial laser hyperthermia for colorectal liver metastases: The effect of thermal sensitization and the use of a cylindrical diffuser tip on tumor necrosis. *J. Clin. Laser Med. Surg.*, **20**: 189–196, 2002.

[17] M.N. Ozisik. *Heat Conduction.* Wiley, New York, 2nd ed., Chapter 14, 1993.

[18] A. Payne, M. Mattingly, R.B. Roemer, E.P. Scott. A model for a thin layer phantom with application to hyperthermia cancer therapy. *Bioengineering Conference, ASME*, **42**: 197–198, 1999.

[19] H.H. Pennes. Analysis of tissue and arterial temperature in the resting human forearm. *J. Appl. Physiol.*, **1**: 93–122, 1948

[20] R.B. Roemer, E.G. Moros, K. Hynynen. A comparison of bioheat transfer and effective conductivity equation predictions to experimental hyperthermia data. *ASME Heat Transfer Division*, **126**: 11–15, 1989.

[21] R.B. Roemer. Optimal power deposition in hyperthermia I. The treatment goal: the ideal temperature distribution: the role of large blood vessels. *Int. J. Hyperthermia*, **7**: 317–341, 1991.

[22] S. Sapareto, W.C. Dewey. Thermal does determination in cancer therapy. *Int. J. Radiation Oncology Bio. Physiol.*, **10**: 787–800.

[23] C. Streffer. Biological basis for the use of hyperthermia in tumor therapy. *Strahlentherapie und Onkologie*, **163**: 416–419, 1987.

[24] N. Tsuda, K. Kuroda. An inverse method to optimize heating conditions in RF-capacitive hyperthermia. *IEEE Transaction on Biomedical Engineering*, **43**: 1029–1037, 1996.

[25] V. Usatoff, N.A. Habib. Update of laser-induced thermotherapy for liver tumors. *Hapatogastroenterology*, **48**: 330–332, 2001.

[26] S. Waldow, P. Morrison, L. Grossweiner. Nd:YAG laser-induced hyperthermia in a mouse tumor model. *Lasers Surg. Med.*, **8**: 510–514, 1988.

[27] M.J. Wang, J.O. Naim, D.W. Rogers, R.J. Lanzafame. The effect of Nd:YAG laser-induced hyperthermia on local tumor recurrence in experimental rat mammary tumors. *Journal of Clinical Medical and Surgery*, **10**: 265–272, 1992.

[28] A.J. Welch, M.J.C. Van Gemert. *Optical Thermal Responses of Laser-Irradiated Tissue.* Plenum Press, New York, 1995.

[29] N.T. Wright. On a relationship between the arrhenius parameters from thermal damage studies. *J. Biomech. Eng.*, **125**: 300–304.

[30] P. Wust, B. Hildebrandt, *et al.* Hyperthermia in combined treatment of cancer. *Lancet Oncol.*, **3**: 487–497, 2002.

[31] L. Zhang, W. Dai, R. Nassar. A numerical modeling for optimizing laser power irradiating on a 3D triple layered cylindrical skin structure. *Numerical Heat Transfer, Part A*, **48**: 21–41, 2005.